James R. Rice and Nouri Levy, "Local Heating by Plastic Deformation at a Crack Tip", in Physics of Strength and Plasticity (published in honor of Egon Orowan), ed. Ali S. Argon, M.I.T. Press, Cambridge, Mass., 1969, pp. 277-293.

Reprinted from:

Physics of Strength and Plasticity

EDITED BY ALI S. ARGON

The M.I.T. Press *Cambridge, Massachusetts, and London, England*

ABSTRACT. Temperature elevations in the plastic zone of a crack are calculated. Stress and strain distributions in nonhardening materials are used, and plastic zones are regarded as distributed sources of heat proportional to the plastic work rate. Results are approximate in that temperature-independent mechanical and thermal properties are assumed and thermal stressing is neglected.

For small-scale yielding and moderately rapid rates, it is found that, under increasing load, the temperature rise at a stationary crack tip is proportional to $K^2/E\sqrt{\rho ckT}$. The same form applies for a running crack, with loading time replaced by the ratio of plastic zone size to velocity v, giving a temperature elevation proportional to $K\sigma_0\sqrt{v}/E\sqrt{\rho ck}$.

Numerical results are given for 2024 aluminum alloy, 6Al–4V titanium alloy, and mild steel. Temperature rises predicted for Krafft's experiments seldom exceed 100°C. These may still be large enough to influence fracture toughness at very fast rates. Assuming that crack tip temperature alone governs fracture toughness, the behavior of the titanium alloy can be explained, and a toughness minimum at slower rates can be predicted for some metals.

20. Local Heating by Plastic Deformation at a Crack Tip

J. R. RICE AND N. LEVY

20.1. Introduction

This paper presents calculations of local temperature elevations accompanying plastic deformation near the tips of stationary and running cracks. The plastic zone at the tip is regarded as the site of heat sources varying in intensity with the distribution of plastic work rates. Calculations are based on some of the known solutions for the stress and strain distribution near a crack tip (Rice 1968, Rice and Rosengren 1968, McClintock and Irwin 1965, Rice 1967, Hutchinson 1968) for elastic perfectly plastic materials. Previous attempts at estimating the temperature rise at the crack tip (Krafft and Irwin 1965, Williams 1965) viewed the plastic zone as the site of a uniform heat generation and were directed at determining whether conditions are more nearly adiabatic or isothermal. Our treatment differs in that the plastic zone grows under increasing load, with plastic work rates (and hence heat generation rates) being far from uniform and tending to very large values within the fracture process zone adjacent to the tip.

The motivation for a precise treatment is the suspicion that such a rise in temperature might be large enough to influence fracture, particularly when loading rates made possible by high speed testing machines are

applied. Eftis and Krafft (1965) observed a minimum in the toughness of mild steel when employing a combined rate scale of reciprocal loading time for stationary cracks and propagation velocity for running cracks. Even when this minimum occurred in the running crack range, the velocity was a small fraction of the wave speed, so it is difficult to believe that inertia effects are responsible. Moreover, results by Krafft and Irwin (1965) on a high-strength 6Al–4V titanium alloy tested at room temperature and below reveal no drop in toughness with rate but rather a steady increase. However, a minimum occurs when the test is made at a higher temperature.

A conventional explanation of fracture rate sensitivity lies with the elevation of flow stress curve with strain rate. Maximum stresses achievable in a nonhardening material will be limited by the initial yield value multiplied by a factor on the order of 2.6 to 3.0 accounting for plane strain constraint so that high strain rates increase local stresses. Strain hardening nullifies this elevation somewhat, for the maximum stress triaxiallity achievable in plane strain increases with strain hardening exponent (Rice and Rosengren 1968, Drucker and Rice 1968) and postyield flow in mild steel reveals a reduction of strain-hardening rate with strain rate. Still on balance, this view of rate sensitivity leads to decreasing toughness with rate and is alone inadequate to explain the observed toughness minimum. Some ambiguities are removed by assuming variations in toughness proportional to corresponding hardening exponent variations, as Krafft has proposed (Krafft 1964, Eftis and Krafft 1965, Krafft and Irwin 1965). This does an admirable job in correlating the behavior of mild steel. As to the behavior of 6Al–4V titanium alloy, Krafft showed that the strain-hardening exponent increases with strain rate, and this could explain the peculiar behavior under increasing loading rate. However, this does not explain the appearance of a minimum toughness for the 180°F test on this alloy (Krafft and Irwin 1965).

As a result of our calculations, it was found that the temperature rise for the titanium alloy is much higher than the rise for steel (by a factor of 6 for the same stress intensity factor). It is, therefore, logical to examine this temperature rise as a possible factor in explaining the difference in the behavior of the titanium alloy and mild steel. The strain-rate elevation of flow stress and local temperature rise will each, in isolation, have opposite effects with the latter, enhancing toughness. They are, of course, both present and highly coupled. For example, isothermal straining will result in a higher flow curve than adiabatic straining at the same rate. Also, thermal expansion accompanying highly localized heating at the crack tip will tend somewhat to counteract the stress-concentrating function of the crack. The energy dissipated in ductile separation of surfaces would presumably increase with temperature of the fracture process zone. In this paper, we do not take all these possibilities into account. We take, rather, the view that loading conditions are prescribed and, with several

approximations, we estimate the associated temperature field. These estimates provide a useful guide for interpreting experimental results, as noted in our concluding sections.

20.2. *Plasticity Models and Assumptions for Temperature Calculations*

For simplicity, we limit attention to cases of a small plane strain plastic zone near a crack tip. The boundary layer formulation of small-scale yielding (Rice 1967, 1968) may then be employed with the characteristic elastic singularity setting asymptotic boundary conditions. Applied load and crack length thus appear only as combined in Irwin's stress intensity factor K (equal to $\sigma_\infty\sqrt{\pi l/2}$ for the Inglis configuration of a crack of length l in an infinite body subjected to the remote tension σ_∞). Further, we employ nonhardening plasticity models with an effective yield stress σ_0 (or τ_0 in shear) and use the plastic work rate from these models as the heat-generation rate for the temperature calculation. This neglects all thermomechanical coupling in affecting the near tip temperature field, except that a numerical value for the yield stress may later be assigned in cognizance of the average temperature and strain rate in the plastic zone.

For constant conductivity and specific heat the equation governing the temperature rise $u = u(x, y, t)$ due to heating by plastic work is

$$\frac{\partial u}{\partial t} = a^2\nabla^2 u + \frac{f(x, y, t)}{\rho c}, \tag{20.1}$$

where $f(x, y, t) = \sigma_{ij}\dot{\varepsilon}^p_{ij}$ is the plastic work rate, ρ the mass density, c the specific heat, k the conductivity, and $a^2 = (k/\rho_c)$ the diffusivity. For partial conversion of work to heat, f should be scaled down proportionally. Carslaw and Jaeger (1959) present the fundamental two-dimensional solution for an instantaneously delivered quantity of heat at a point in the infinite xy plane. Taking our plastic work rate $f(x, y, t)$ as a continuous distribution of heat sources and superposing, the solution to Equation 20.1 is

$$u(x, y, t) = \int_0^t \left\{ \iint_{A_P(\tau)} \frac{f(\xi, \eta, \tau)}{\rho c} \exp\left[-\frac{(x-\xi)^2 + (y-\eta)^2}{4a^2(t-\tau)} \right] d\xi\, d\eta \right\} \times \frac{d\tau}{4\pi a^2(t-\tau)} \tag{20.2}$$

Here $A_P(t)$ is the plastically deforming region at time t. It is appropriate to use the fundamental solution for an uncracked plane here, since the work rate f will be symmetric about the crack line so as to nullify any heat conduction across the crack surface.

This integral is the desired form of solution to the temperature equation for the rapid loading of a stationary crack. It is inconvenient for a running

crack. A suitable approximation to the latter case would regard the crack velocity and plastic zone size as constant (for purposes of temperature calculation only) so that a plastic work rate independent of time, say $g(x, y) = \sigma_{ij}\dot{\varepsilon}^p_{ij}$, results referred to a system of coordinates moving with the crack tip. Again the solution is given by superposing heat sources, this time employing the fundamental solution (Carslaw and Jaeger 1959) for a point source moving at constant speed v equal to the crack velocity. There results

$$u(x, y) = \iint_{A_P} \frac{g(\xi, \eta)}{2\pi k} \exp\left[-\frac{v(x-\xi)}{2a^2}\right] \times K_0\left\{\frac{v}{2a^2}[(x-\xi)^2 + (y-\eta)^2]^{1/2}\right\} d\xi\, d\eta. \tag{20.3}$$

Here A_P is the plastically deforming region in the moving coordinates and K_0 is the modified Bessel function of the second kind.

The functions $f(x, y, t)$ and $g(x, y)$ are determined from the crack-tip plasticity model employed. An approximate nonhardening plane strain analysis for small-scale yielding at a stationary crack tip has been given by Rice (1968), as based on the slip-line theory and his path-independent line integral. Plastically deforming regions result in centered fans above and below the crack tip, so that if a polar coordinate system is chosen with origin at the tip with $\theta = 0$ being the line ahead of the crack, the extent of the plastic region is approximately

$$R_P(\theta) = \omega \cos 2(\theta - \pi/2) \quad \text{where} \quad \omega = \frac{3(1-\nu)}{\sqrt{2}(2+\pi)}\left(\frac{K}{2\tau_0}\right)^2. \tag{20.4}$$

Here ω is the maximum dimension of the plastic zone and $R_P(\theta)$ is the distance from the crack tip to the elastic-plastic boundary along a ray at angle θ, the boundary cutting into the tip along 45-deg boundaries of the centered fans. The associated plastic work rate at points within the plastic zone may be obtained from Rice (1968) as

$$f(r, \theta, t) = \frac{d}{dt}\left[\frac{\tau_0^2}{G}\frac{R_P(\theta)}{r}\right] = \frac{\tau_0^2}{Gr}\cos 2(\theta - \pi/2)\frac{d\omega}{dt} \quad \text{for} \quad r < R_P(\theta) \tag{20.5}$$

(G is the elastic shear modulus).

No analogous tensile plasticity model is available for an advancing crack. We therefore employ the simple Dugdale (1960) model which represents yielding by essentially viewing the crack as longer by a length equal to the plastic zone size, with the plastic separation displacements

of the extended crack surface being opposed by the tensile yield stress σ_0. The small-scale yielding plastic zone size then is

$$\omega = \frac{\pi}{8}\left(\frac{K}{\sigma_0}\right)^2. \tag{20.6}$$

Separation displacements are the same whether the crack is moving or not. From the expressions given in Rice (1967) one may compute the Dugdale plastic work rate in plane strain for a stationary crack as

$$f(x, y, t) = \frac{4(1-\nu)\sigma_0^2}{\pi G}\left(1 - \frac{x}{\omega}\right)^{1/2} \delta_D(y)\frac{d\omega}{dt}, \quad \text{for} \quad 0 < x < \omega. \tag{20.7}$$

Here the coordinate origin is at the tip with the x axis extending directly ahead, and $\delta_D(\ldots)$ is the Dirac delta function resulting from the displacement discontinuity in the plastic zone. For the running-crack case, we take the coordinate origin at the moving tip with the x axis again directly ahead. Presuming the plastic zone to remain fixed in size as the crack advances, the work rate is computed from Rice (1967) as

$$g(x, y) = \frac{2(1-\nu)\sigma_0^2}{\pi G}\log\left[\frac{1 + (1 - x/\omega)^{1/2}}{1 - (1 - x/\omega)^{1/2}}\right]\delta_D(y)v, \quad \text{for} \quad 0 < x < \omega. \tag{20.8}$$

Were the growth of the plastic zone with crack length taken into account, the resulting work rate would be the sum of Equations 20.7 and 20.8. Thus our treatment of the running-crack case as steady-state problem is justified as long as the crack speed v greatly exceeds the zone growth rate $d\omega/dt$, which is satisfied by definition for small-scale yielding. The Dugdale model is most appropriate for plane stress rather than plane strain, and this poses an important limitation on our running-crack results as noted later.

20.3. Temperature Rise at the Tip of a Stationary Crack

When the plastic work rate $f(r, \theta, t)$ is represented in polar coordinates with the crack tip at the coordinate origin, Equation 20.2 gives the crack-tip temperature rise after loading from times 0 to t as

$$u = \int_0^t \left\{ \iint_{A_P(\tau)} \frac{f(r, \theta, \tau)}{\rho c} \exp\left[-\frac{r^2}{4a^2(t-\tau)}\right] r\, d\theta\, dr \right\} \frac{d\tau}{4\pi a^2(t-\tau)}. \tag{20.9}$$

Note that only the angular average (in θ) of the work rate contributes. This is the reason why the two plasticity models we consider, involving

very different yielding patterns, lead to similar results. Inserting the work rate for the plane-strain slip-line model (Equation 20.5) and integrating in θ,

$$u = \frac{\tau_0^2}{2\pi k G}\int_0^t \left\{\int_0^{\omega(\tau)} \sqrt{1-[r/\omega(\tau)]^2}\,\exp\left[-\frac{r^2}{4a^2(t-\tau)}\right]dr\right\} \times \frac{d\omega(\tau)}{d\tau}\frac{d\tau}{t-\tau}. \tag{20.10}$$

Here the time variation of $\omega(\tau)$ is determined through Equation 20.4 in terms of the imposed time variation in the stress-intensity factor. An identical formula results for the Dugdale model, except that the τ_0^2 in front is replaced by $2(1-\nu)\sigma_0^2/\pi$ and the r/ω appearing within the square root sign is then raised only to the first power.

Dimensionless variables are now convenient. Let T denote the time at which the maximum load is reached on a cracked specimen, let $K_{\max}$ be the corresponding stress intensity and $\omega_{\max}$ the plastic zone dimension resulting at $K_{\max}$. Define

$$\alpha = t/T, \qquad \Omega(\alpha) = \omega(t)/\omega_{\max} = [K(t)/K_{\max}]^2, \qquad R = r/\omega_{\max} \tag{20.11}$$

as dimensionless time, plastic zone size, and distance, respectively. Further let

$$\delta = \frac{2a\sqrt{T}}{\omega_{\max}} \tag{20.12}$$

be a dimensionless measure of the shortness of time to maximum load. Then Equation 20.10 for the crack-tip temperature rise at the time of maximum load may be put in the form

$$u = u_c\, h(\delta), \tag{20.13}$$

where u_c has temperature dimensions and may be expressed in terms of loading time and maximum load, and $h(\delta)$ is a dimensionless function depending on the manner of load variation with time. For the plane-strain slip-line model

$$u_c = \sqrt{\frac{2}{\pi}}\frac{1}{2+\pi}\frac{(1-\nu^2)K_{\max}^2}{E\sqrt{\rho c k T}} = 0.156\,\frac{(1-\nu^2)K_{\max}^2}{E\sqrt{\rho c k T}}, \tag{20.14}$$

(E is Young's modulus), and for the Dugdale model,

$$u_c = \frac{2}{3\sqrt{\pi}}\frac{(1-\nu^2)K_{\max}^2}{E\sqrt{\rho c k T}} = 0.377\,\frac{(1-\nu^2)K_{\max}^2}{E\sqrt{\rho c k T}}. \tag{20.15}$$

We interpret u_c shortly. The function $h(\delta)$ for the plane-strain slip-line model is given by the double integral

$$h(\delta) = \frac{3}{4\sqrt{\pi}} \int_0^1 \frac{\Omega'(\alpha)}{\sqrt{1-\alpha}} \int_0^{\Omega(\alpha)} \frac{\sqrt{1-[R/\Omega(\alpha)]^2}}{\delta\sqrt{1-\alpha}} \times \exp\left[-\frac{R^2}{\delta^2(1-\alpha)}\right] dR\, d\alpha. \tag{20.16}$$

The same formula applies for the Dugdale model, eccept that the $R/\Omega(\alpha)$ ratio within the square root sign is raised to only the first power.

3.1 *Rapid Loading*

Consider a very short time to attainment of maximum load so that δ (Equation 20.12) is small compared to unity. The situation is approximated by seeking the limit of $h(\delta)$ as $\delta \to 0$. In that limit the entire contribution to the integral on R in Equation 20.16 is shifted to the origin $R = 0^+$. The integrand becomes infinite there, but not the integral itself which approaches the form of the half-infinite normal error integral of value $\sqrt{\pi/2}$. Hence, in the short loading time limit the crack-tip temperature rise for both models is

$$u = \frac{3}{8} u_c \int_0^1 \frac{\Omega'(\alpha)}{\sqrt{1-\alpha}}\, d\alpha. \quad \text{for } \delta \ll 1. \tag{20.17}$$

If the applied load rises linearly with time up to maximum load, $\Omega(\alpha) = \alpha^2$ by Equation 20.11 and the integral turns out to have the value 8/3 so that the temperature rise at maximum load is

$$u = u_c \quad \text{(constant loading rate and } \delta \ll 1\text{)}. \tag{20.18}$$

Thus our arrangement of Equation 20.13, with the temperature rise referenced to this short time constant-rate limit as given by Equations 20.14 and 20.15. One may also show from Equation 20.17 that the short-time limit temperature elevation is $3u_c/4$ if the load rises as $t^{1/2}$ and $6u_c/5$ if the load rises at $t^{3/2}$.

The function $h(\delta)$ or u/u_c is plotted as a function of δ in Figure 20.1, as obtained through numerical integration of Equation 20.16 for the special case of the applied load rising linearly with time. It is seen that $h(\delta)$ tends very rapidly to unity as δ or $2a\sqrt{T}$ becomes small. In other words, the temperature at the crack tip, for a given material, becomes proportional to u_c which is inversely proportional to loading time, as can be seen from Equation 20.14. It is interesting to note that the thermal properties influencing the temperature at the crack tip appear in the term $1/\sqrt{k\rho c}$.

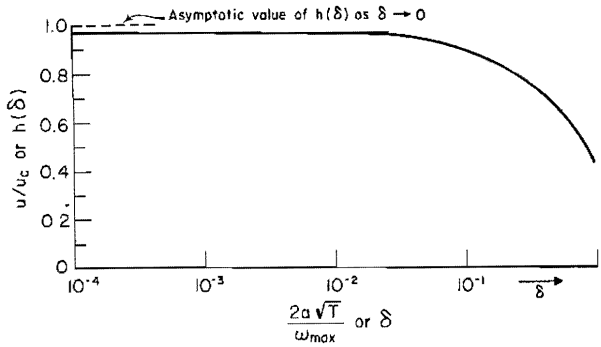

FIGURE 20.1. The value of the function $h(\delta)$ for constant rate of loading (temperature rise at stationary crack tip $= u_c\, h(\delta)$).

3.2 *Temperature Distribution Near the Tip*

It is clear that the maximum temperatures occurring at the tip (Equations 20.13 to 20.18) will hold over a highly localized region. From the presence of the thermal conductivity k in expressions for u_c, one might conclude that it is never meaningful to speak of "adiabatic conditions" at the tip even for very short loading times. Nevertheless, adiabatic conditions may result a short distance away from the tip. The $1/r$ strain singularity of the slip-line model suggests that the temperature gradient will then be quite steep. The gradient is, of course, unrealistically steep along the plastic zone of the Dugdale model due to the concentration of deformation in a band. This dependence on artificial localization of the deformation is alleviated by focusing on the average temperature on a circle of radius r_0:

$$\bar{u}(r_0, t) = \frac{1}{2\pi} \int_{-\pi}^{+\pi} u(r_0, \phi, t)\, d\phi. \tag{20.19}$$

Upon expressing both the source points and response point in polar coordinates, the general solution of Equation 20.2 becomes

$$u(r_0, \phi, t) = \int_0^t \left\{ \iint_{A_P(\tau)} \frac{f(r, \theta, \tau)}{\rho c} \exp\left[- \frac{r^2 - 2rr_0 \cos(\phi - \theta) + r_0^2}{4a^2(t - \tau)} \right] r\, d\theta\, dr \right\} \times \frac{d\tau}{4\pi a^2 (t - \tau)} \tag{20.20}$$

Averaging as in Equation 20.19 converts the ϕ-dependent part of the exponential term to a modified Bessel function of the first kind (McLachlan 1961) so that

$$\bar{u}(r_0, t) = \int_0^t \left\{ \iint_{A_P(\tau)} \frac{f(r, \theta, \tau)}{\rho c} \exp\left[- \frac{r^2 + r_0^2}{4a^2(t - \tau)} \right] I_0\left[\frac{rr_0}{2a^2(t - \tau)} \right] r\, d\theta\, dr \right\} \times \frac{d\tau}{4\pi a^2 (t - \tau)} \tag{20.21}$$

This equation is identical in form to Equation 20.9 in that only the angular average of the work rate contributes, as desirable in view of uncertainties in the models. The remaining steps are identical to the progression from Equations 20.9 to 20.16 so that the average temperature on a circle of radius r_0 at the time T of loading to a plastic zone dimension ω_{max} is

$$\bar{u} = \frac{3}{4\sqrt{\pi}} u_c \int_0^1 \frac{\Omega'(\alpha)}{\sqrt{1-\alpha}} \int_0^{\Omega(\alpha)} \frac{\sqrt{1-[R/\Omega(\alpha)]^2}}{\delta\sqrt{1-\alpha}} \times \exp\left[-\frac{R^2+R_0^2}{\delta^2(1-\alpha)}\right] I_0\left[\frac{2RR_0}{\delta^2(1-\alpha)}\right] dR\, d\alpha \tag{20.22}$$

where $R_0 = r_0/\omega_{max}$ and the remaining notation is as given above. This reduces to the crack-tip form of Equations 20.13 and 20.16 when $R_0 = 0$. Here the square power on $R/\Omega(\alpha)$ applies again for the plane-strain slip-line model, with a power of unity for the Dugdale model.

One need only consider small values of r_0 since temperature rises will be entirely negligible at distances from the tip comparable to the plastic zone dimension. For example, the plane-strain slip-line model estimates the maximum plastic shear strain on the circle $r_0 = \omega_{max}/10$ as only $9\gamma_0$. Further, negligible temperature elevations will occur throughout the zone unless the dimensionless loading time δ is small. When both R_0 and δ are small compared to unity, the major contribution of the integral on R is localized around R_0 and the integrand falls off rapidly to zero due to $\exp[-R^2/\delta^2(1-\alpha)]$. Thus one introduces negligible error (and zero in the limit as both δ and $R_0 \to 0$) by replacing the term $\sqrt{1-[R/\Omega]^2}$ by unity and the upper limit $\Omega(\alpha)$ by ∞. Consequently, the temperature elevation then depends on R_0 and δ only through the combination R_0/δ:

$$\bar{u} = u_c\, p\left(\frac{R_0}{\delta}\right) = u_c\, p\left(\frac{r_0}{\delta\omega_{max}}\right) = u_c\, p\left(\frac{r_0}{2a\sqrt{T}}\right), \quad \text{for} \quad \delta \quad \text{and} \quad R \ll 1, \tag{20.23}$$

where the function $p(\ldots)$ is defined by

$$p(\lambda) = \frac{3}{4\sqrt{\pi}} \int_0^1 \frac{\Omega'(\alpha)}{1-\alpha} \int_0^\infty \exp\left[-\frac{\lambda^2+\mu^2}{1-\alpha}\right] I_0\left[\frac{2\lambda\mu}{1-\alpha}\right] d\mu\, d\alpha. \tag{20.24}$$

Equation 20.23 reveals the parameter $2a\sqrt{T}$ as the size scale over which temperatures comparable to the tip value will result.

If the loading time is so short that $2a\sqrt{T}$ is small compared to the radius r_0 of interest, the asymptotic formula (McLachlan 1961) $I_0(z) = (2\pi z)^{-1/2} e^z$ may be employed for the Bessel function so that $p(\lambda) \approx 3/8\sqrt{\pi\lambda}$, and

$$\bar{u} \approx \frac{3}{8\sqrt{\pi}} u_c \frac{2a\sqrt{T}}{r_0} \quad \text{for} \quad r_0 \gg 2a\sqrt{T}. \tag{20.25}$$

This is independent of the loading time (since $u_c \sim 1/\sqrt{T}$) and could have been written down immediately from adiabatic considerations. The function $p(\lambda)$ has been evaluated numerically for the case of a linearly rising load ($\Omega = \alpha^2$), and the angular averaged temperature at r_0 is shown in dimensionless form as $\bar{u}/u_c$ vs. $r_0/2a\sqrt{T}$ (or $r_0/\delta\omega_{max}$) in Figure 20.2.

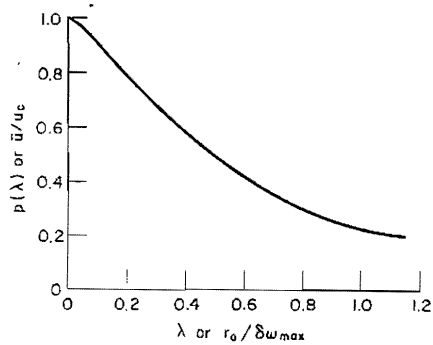

FIGURE 20.2. The value of the function $p(\lambda)$ or $\bar{u}/u_c$. Nomenclature: $\bar{u}$ = average temperature along a circle with radius r_0 from the crack tip; u_c = characteristic temperature as defined; $\delta = 2a\sqrt{T}/\omega_{max}$; $a^2 = k/\rho c$ or diffusivity; T = loading time; ω_{max} = maximum length of plastic zone.

Finite geometry changes occurring through blunting of the crack tip will limit conditions at which sharp crack temperature predictions are considered acceptable. We may approximate the tip temperature in a rough way by taking r_0 as half the tip opening displacement, which is $r_0 = 4(1-\nu^2)\varepsilon_0\,\omega_{max}/\pi \approx \varepsilon_0\,\omega_{max}$ for the Dugdale model ($\varepsilon_0 = \sigma_0/E$ is the initial yield strain). This correction would estimate the tip temperature as

$$u \approx u_c p\left(\frac{\varepsilon_0}{\delta}\right), \tag{20.26}$$

so that our previous formulae apply if δ is comparable to or larger than ε_0. An upper limit to the achievable tip temperature is then given by Equation 20.24, when the loading time is so short that δ is small compared to the initial yield strain. Employing Equations 20.15 and 20.16, this upper limit is

$$u \approx \sigma_0/\pi\rho c. \tag{20.27}$$

The numerical factor of π is probably not very accurate, but otherwise the form is plausible as it represents the adiabatic temperature rise accompanying a strain on the order of unity. With the π factor, this value is 120°C for the titanium alloy 6Al–4V, and 60°C for mild steel and 80°C for aluminum 2024, for values σ_0 as obtained in "static" tensile tests. If, however, the effect of the high strain rates is to be taken into account,

these upper bounds should be scaled up in proportion to the increase in the yield strengths. A figure of 3 is usually taken for steel, and the upper limit is 180°C.

20.4. Temperature Rise at a Running Crack Tip

In contrast to the stationary crack for which the tip temperature rise is insensitive to the details of the work rate distribution (Equation 20.9), a strong directionality is suggested by the exponential term of the running crack solution in Equation 20.3. The Dugdale model predicts an unrealistically large concentration of plastic work directly ahead of the crack tip. While the lack of more accurate advancing crack models forces a limitation to this case, it is expected that predicted temperatures will somewhat exceed actual values.

Setting $x = y = 0$ in Equation 20.3 so as to describe the temperature rise at the running crack tip, employing the Dugdale work rate of Equation 20.8 and integrating in η, one obtains

$$u = \frac{(1-\nu)\sigma_0^2 v}{\pi^2 G k} \int_0^{\omega} \log\left[\frac{1+(1-\xi/\omega)^{1/2}}{1-(1-\xi/\omega)^{1/2}}\right] \exp\left(\frac{v\xi}{2a^2}\right) K_0\left(\frac{v\xi}{2a^2}\right) d\xi. \tag{20.28}$$

Here ω is the plastic zone size as given by Equation 20.6 and v is the crack speed. Let $R = \xi/\omega$ be a dimensionless distance and define

$$m = \frac{v\omega}{2a^2} \tag{20.29}$$

as a dimensionless measure of the rapidity of crack speed. Then Equation 20.19 may be placed in a form analogous to the stationary crack case as

$$\frac{u}{u_c} = h(m) = \frac{\sqrt{m}}{\pi\sqrt{2\pi}} \int_0^1 \log\left[\frac{1+(1-R)^{1/2}}{1-(1-R)^{1/2}}\right] \exp(mR) K_0(mR)\, dR.$$

The characteristic temperature for the running crack is

$$u_c = \frac{\sqrt{\pi}}{2} \frac{(1-\nu^2)K^2}{E\sqrt{\rho c k}} \sqrt{\frac{v}{\omega}} = 0.886 \frac{(1-\nu^2)K^2}{E\sqrt{\rho c k}} \sqrt{\frac{v}{\omega}}. \tag{20.31}$$

This value of u_c (which will shortly be shown to be the large m limit) is in the same form as Equation 20.15, except that the velocity over plastic zone size replaces reciprocal loading time and the numerical factor is larger. Note that here a dependence on yield stress (through ω) results, in contrast to the stationary crack case. In terms of σ_0,

$$u_c = \sqrt{2}\, \frac{(1-\nu^2)K\sigma_0\sqrt{v}}{E\sqrt{\rho c k}} = 1.414 \frac{(1-\nu^2)K\sigma_0\sqrt{v}}{E\sqrt{\rho c k}}. \tag{20.32}$$

The high velocity case is handled by computing the limit of $h(m)$ as $m \to \infty$. For large values of its argument the Bessel function behaves as (McLachlan 1961) $K_0(z) \to (\pi/2z)^{1/2} e^{-z}$. Inserting this form for $K_0(mR)$ as $m \to \infty$ in Equation 20.30, one finds that $h(\infty) = 1$ so that the u_c of Equations 20.31 and 20.32 is the large velocity form for the tip temperature. The ratio u/u_c is plotted in Figure 20.3 as a function of m. The function

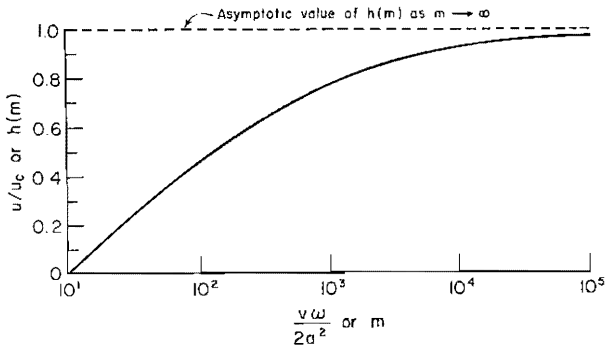

FIGURE 20.3. The value of the function $h(m)$ (temperature rise at the tip of a running crack $= u_c\, h(m)$).

$h(m)$ tends asymptotically to 1.0 as $m \to \infty$. Therefore, for very high values of m (or $v\omega/2a^2$), the temperature at the tip of the crack is directly proportional to u_c or the square root of the velocity. Again, the thermal properties influence the temperature rise through the term $1/\sqrt{k\rho c}$.

20.5. Numerical Results

The magnitude of the temperature rise at the tip of a stationary or a running crack is shown as a function of the stress-intensity factor for three materials (Figures 20.4 and 20.5). The materials, mechanical, and

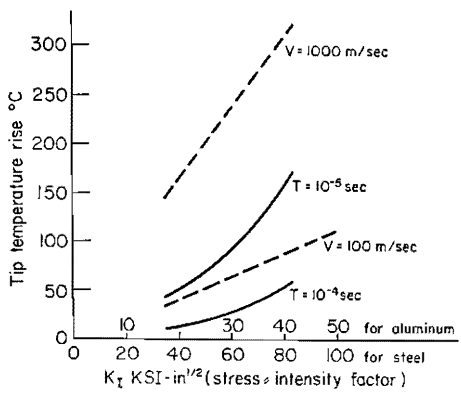

FIGURE 20.4. Temperature dependence on stress intensity factor K_1 for aluminum 2024 alloy with Y–S 30 KSI, and mild steel with Y–S 60 KS_I.

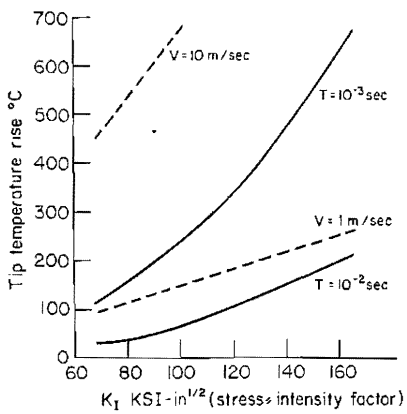

FIGURE 20.5. Dependence of root temperature on stress-intensity factor, for Titanium-6 Al-4V alloy with Y–S 120 KSI.

thermal properties at room temperature relevant to the calculations are taken as shown in the following table.

Yield Strength ksi	Thermal Conductivity cal/sec°C	Specific Heat cal/g°C	Diffusivity cm^2/sec	$\sqrt{k\rho c}$ $cal/cm^2°C\,sec^{1/2}$
		2024 Aluminum Alloy		
30	0.410	0.185	0.85	0.475
		Mild Steel		
60	0.143	0.10	0.20	0.330
		6Al-4V Titanium Alloy		
120	0.018	0.13	0.032	0.110

Noting that the temperature rise for a given K_I is proportional to $1/\sqrt{T}$ (Equation 20.24) or $\sqrt{v}$ (Equation 20.23) for the stationary crack and the running crack, respectively, it is easy to calculate the rise in temperature for loading times or propagation velocities other than those shown in the figures.

It should be noted that the results for v = constant for the running crack depend on the yield strength chosen, since the rise in temperature is proportional to $\sigma_0 K$. In Figures 20.4 and 20.5, the yield strengths used are those obtained from a standard tensile test. Therefore, if the rise in yield strength due to the very high strain rates such as occur at the tip of a running crack is taken into account, the results in Figures 20.4 and 20.5 for the running crack should be increased proportionately to the increase in the yield strength.

To have an idea on the magnitude of the temperature rise in actual experiments, the data from Krafft and Irwin (1965) was considered. For example, Figure 5 of Krafft and Irwin shows the variation of the critical stress-intensity factor with loading time for 6Al-4V titanium alloy. The critical stress-intensity factor is equal to 70 ksi$\sqrt{\text{in}}$ at loading time $T = 10^{-3}$ sec, for a specimen tested at 180°F. For this point, the temperature rise at the tip of the crack is calculated to be 120°C. The temperature rise at the point of minimum critical-stress intensity factor is only 10°C.

In Figure 6 of Krafft and Irwin (1965) for mild steel the temperature rise at the minimum critical-stress intensity factor for the test run at −320°F is less than 1°C. However, at the highest stress-intensity rate in the same test, the rise is estimated at 50°C. As to the running crack, the rise in temperature is calculated for the various velocities of propagation as shown below:

Velocity of Propagation	*Temperature Rise*
100 ft./sec.	80°C
1000 ft./sec.	400°C
3000 ft./sec.	1400°C

Being calculated from the Dugdale model, these are probably overestimates. Also, we have not assessed the role of tip blunting in providing an effective upper limit (to parallel Equation 20.27) for the running-crack case.

Although no data are available for the propagating crack in 6Al-4V titanium alloy, the temperature rise is twelve times as high as for mild steel for comparable stress-intensity factors and velocities of propagation.

20.6. Influence of Local Heating at the Tip of a Stationary Crack on Toughness

As can be seen from the preceding results, the rise in temperature at the tip of a stationary crack is not huge even at very high loading rates. Nowhere in the data of Krafft and Irwin (1965) does this rise exceed 120°C. However, whether this local temperature increase is to be considered as "small" or "large" depends on its effect on the behavior in fracture. For the moment, let us assume that a local heating at the tip to a temperature u will result in a behavior similar to that of a specimen at a uniform temperature u. This seems to be a plausible assumption, since fracture being a local phenomenon, the mechanical properties at or near the tip govern.

It is generally observed that increasing the temperature of a notched specimen increases the toughness for a given loading rate. Moreover, as the loading rate is increased, the toughness usually decreases for a given specimen temperature. If, therefore, we consider the influence of loading rate and the temperature rise at the tip which increases with loading rate,

we will have two opposing factors acting simultaneously. At very high loading rates and, hence, very high average strain rates near the tip, the mechanical properties tend to be little sensitive to further increases in strain rates (Marsh and Campbell 1963). At this stage, the local temperature rise dependence on increased loading rate will perhaps emerge as the sole important factor in affecting toughness. Beyond this stage, therefore, toughness will increase as the loading rate is increased. It follows that materials which show a reduction in toughness versus loading rates, at low loading rates, will exhibit a minimum toughness at critical loading rate beyond which toughness will increase as the loading rate is increased.

Factors such as lower testing temperatures which reduce the sensitivity of mechanical properties to strain rates and at the same time enhance the term $1/\sqrt{k\rho c}$ (which accounts for the temperature rise) will shift the critical loading rate (point of minimum toughness) to lower values of loading rates. Moreover, if the sensitivity to strain rate is small, such as for F.C.C. metals, and if the term $1/\sqrt{k\rho c}$ is large, the critical loading rate can be extremely small and might be suppressed altogether. This is perhaps the case for the titanium alloy 6Al–4V, which shows a rising toughness versus loading rate when tested at room temperature or below. However, as the testing temperature is increased, the sensitivity to strain rates is enhanced simultaneously with a reduction of the term $1/\sqrt{k\rho c}$, and thus a reduction in toughness versus loading rate should be observed up to a critical loading rate, beyond which toughness will increase as the loading rate is increased.

The assumption that a given local temperature rise affects toughness to the same degree as an equal uniform rise in temperature of the whole specimen (at very high loading rates), suggests a method of determining the dependence of toughness on loading rate for a given test temperature when the toughness at various test temperatures at a given loading rate is known. Suppose, as in Figure 20.6, that the toughness for test temperatures $u(1)$ and $u(2)$ at loading time T_1 is known. We assume that at the given loading time, the average strain rate near the tip is high enough so that the effect of further increase in strain rates on toughness is negligible. The temperature rises $\Delta u(1)$ at (1), and $\Delta u(2)$ at (2) can be calculated. To reach point (3), where $K(3) = K(1)$, the temperature at the tip of the crack must be equal to that at 1. In other words,

$$u(2) + \Delta u(3) = u(1) + \Delta u(1) \quad \text{or} \quad \Delta u(3) = u(1) - u(2) + \Delta u(1).$$

Since $\Delta u(3)/\Delta u(1) = \sqrt{T_1}/\sqrt{T_3}$, one can calculate T_3 and the point (3) can be thus located. Thus the toughness versus loading time at a temperature $u(2)$ can be predicted from the variation of toughness versus loading time at $u(1)$ if toughness versus temperature at a given loading time is known. Using the data of Krafft and Irwin (1965) for the 6Al-4V titanium alloy

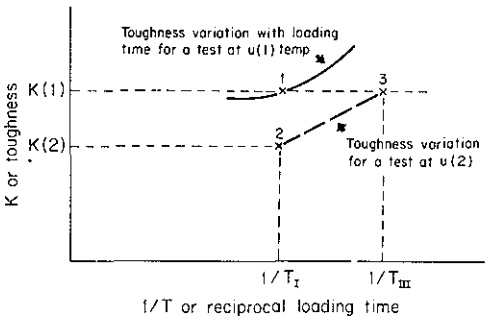

FIGURE 20.6. Method for deriving toughness vs. loading time for a test at $u(2)$ when behavior is known at $u(1)$. Nomenclature: (2): point on the curve for a test at $u(2)$ when $u(2) < u(1)$; $\Delta u(1)$: elevation of temperature at crack tip for point (1); $\Delta u(2)$:elevation of temperature at crack tip for point (2); T_{III} : loading time at which the toughness reaches the value $K(1)$;

$$T_{III} = \left[\frac{\Delta u(1)}{u(1) - u(2) + \Delta u(1)}\right]^2 T_I .$$

tested at 180°F, the predicted toughness versus loading rate for the test at 80°F was found to be equal to the one reported in the reference. Point (1) is taken as the point of minimum toughness for the 180°F test; point (2) is the point on the 80°F test at the same loading time as point (1), and point (3) is the toughness at the time of loading 10^{-3} seconds on the 80°F test.

Insufficient data are available for a more thorough quantitative test of this method. Nevertheless, a qualitative understanding of experimental data does result as noted above.

This research was supported by the Office of Naval Research under Contracts Nonr 562(20) and N00014–67–A–0191–003.

REFERENCES

Carslaw, H. S., and J. C. Jaeger, 1959, *Conduction of Heat in Solids*, Oxford: Clarendon Press. 2dn ed.

Drucker D. C., and J. R. Rice, 1969, *Eng. Fract. Mech.*, in press.

Dugdale, D. S., 1960, *J. Mech. Phys. Sol.*, **8**, 100.

Eftis, J., and J. M. Krafft, 1965, *J. Basic Eng.*, **87**, 257.

Hutchinson, J. W., 1968, *J. Mech. Phys. Sol.*, **16**, 13.

Krafft, J. M., 1964, *Appl. Mat. Res.*, **3**, 88.

Krafft, J. M., and G. R. Irwin, 1965, *Symposium on Fracture Toughness Testing*, STP No. 381, Philadelphia: ASTM, p. 114.

Marsh, K. J., and J. D. Campbell, 1963, *J. Mech. Phys. Sol.*, **11**, 49.

McClintock, F. A., and G. R. Irwin, 1965, *Symposium on Fracture Toughness Testing*, STP No. 381, Philadelphia: ASTM, p. 84.

McLachlan, N. W., 1961, *Bessel Functions for Engineers*, Oxford: Clarendon Press.

Rice, J. R., 1967, *Symposium on Fatigue Crack Growth*, STP No. 415, Philadelphia: ASTM, p. 247.

Rice, J. R., 1968, *J. Appl. Mech.*, **35**, 379.

Rice, J. R., and G. F. Rosengren, 1968, *J. Mech. Phys. Sol.*, **16**, 1.

Williams, J. G., 1965, *Appl. Mat. Res.*, **4**, 104.